Radiation Physics and Chemistry 211 (2023) 111047

Contents lists available at ScienceDirect

Radiation Physics and Chemistry

journal homepage: www.elsevier.com/locate/radphyschem

In-situ preparation of chemically-crosslinked polyvinylpyrrolidone gel polymer electrolyte for lithium ion battery via room-temperature electron beam-induced gelation

Joon-Yong Sohn [a,b], Ji Hoon Choi [a], Pyeong-Wook Kim [a,c], In-Tae Hwang [a], Junhwa Shin [a], Chan-Hee Jung [a,*], Young-Moo Lee [b,**]

[a] Advanced Radiation Technology Institute, Korea Atomic Energy Research Institute, 29 Geumgu-gil, Jeongeup, Jeollabuk-do, 56212, Republic of Korea
[b] Department of Energy Engineering, Hanyang University, 222 Wangsimni-ro, Seongdong-gu, Seoul, 04763, Republic of Korea
[c] Department of Chemistry & Institute of Biological Interfaces, Sogang University, 35 Baekbeom-ro, Mapo-gu, Seoul, 04107, Republic of Korea

ARTICLE INFO

Handling Editor: Dr. Jay Laverne

Keywords:
In-situ gelation
Electron beam irradiation
Gel polymer electrolyte
Lithium ion batteries

ABSTRACT

In this research, we report an initiator-free and room-temperature 2.5 MeV electron beam (EB)-induced gelation strategy to in-situ create polyvinylpyrrolidone-based gel polymer electrolytes (PVP-GPEs) in a fully-assembled lithium ion battery (LIB). A radiation-sensitive liquid precursor consisting of 1-vinyl-2-pyrrolidone (VP), poly (ethylene glycol) diacrylate (PD), and $LiClO_4$ liquid electrolyte (LE) was effectively converted to freestanding PVP-GPEs even at an absorbed dose of 2 kGy (Irradiation time of 6 s). The formed GPE at the absorbed dose of 2 kGy exhibited good thermal stability and mechanical integrity while providing good electrochemical oxidative stability (up to 4.7 V) and ion conductivity (2.03×10^{-3} S/cm at 25 °C). Moreover, the $LiCoO_2$/PVP-GPE/graphite coin cell in-situ prepared at the absorbed dose of 2 kGy showed comparable retention capacity to that of an LE-based coin cell after 50 cycles. The findings of this study suggest that the proposed in-situ quick EB-induced gelation strategy (without use of an initiator and thermal treatment) could be a scalable way to allow high-throughput production of reasonably performing and safe LIBs.

1. Introduction

Lithium-ion batteries (LIBs), which are promising portable energy storage devices, have attracted significant interest during the past two decades because of their high energy density, excellent cycle ability, and the absence of a memory effect (Chen et al., 2021; Kim et al., 2019; Service, 2019). Recently, applications of LIBs have been extended from portable electronics to large-scale energy storage for electric vehicles, aviation technology, and smart grids (Deng et al., 2020; Duan et al., 2020; Zubi et al., 2018). An LIB consists of two electrodes, a separator, and an electrolyte. Among these components, the safety of the conventionally-used liquid electrolyte (LE), which provides ion transport pathways, is one of the key issues to achieve large-scale LIBs (Chen et al., 2017; Duan et al., 2020; Schmuch et al., 2018). Due to their high flammability and corrosiveness, LE-based LIBs have significant potential dangers, such as combustibility and impact or heat-induced explosion (Cavers et al., 2022; Cheng et al., 2018; Xu, 2014). To resolve this safety problem, solid-like gel polymer electrolytes (GPEs), a promising alternative for commercialization, have been widely studied over the last few decades due to their attractive characteristics (Kuo et al., 2016; Shim et al., 2017; Zhu et al., 2016). GPEs offer appealing characteristics, including good ion conductivity (two orders of magnitude greater than that of solid electrolyte) and better stability than that of LEs (Lv et al., 2018; Rao et al., 2012; Wang et al., 2017b; Zheng et al., 2014 Zhu et al., 2015).

GPEs generally have been prepared by two main approaches, physical and chemical gelation (Cho et al., 2019; Ma et al., 2022; Song et al., 1999). Physical gelation is performed by immersing solid polymer matrices into a LE, offering good processibility and performance for manufacturing LIBs (Cho et al., 2019). However, this approach accompanies difficulty in control of leakage and severe long-term mechanical deformation (Ma et al., 2022; Wang et al., 2017a). On the other hand, chemical gelation by crosslinking or polymerization of a monomer and crosslinker in the presence of LE has been preferred because it provides

* Corresponding author.
** Corresponding author.
E-mail addresses: jch@kaeri.re.kr (C.-H. Jung), ymlee@hanyang.ac.kr (Y.-M. Lee).

https://doi.org/10.1016/j.radphyschem.2023.111047
Received 14 March 2023; Received in revised form 16 May 2023; Accepted 18 May 2023
Available online 19 May 2023

outstanding long-term LE retention capability and mechanical durability (Ma et al., 2022). Chemical gelation has mostly been carried out by thermal treatment (Choi et al., 2014a; Lee et al., 2014; Oh et al., 2011; Shi et al., 2014; Woo et al., 2018; Zheng et al., 2014; Zhou et al., 2014, 2015). However, the thermal treatment requires long time and high temperatures (potentially leading to performance degradation and gas emission-induced cell expansion). An alternative to thermal treatment is UV irradiation to avoid heat-induced damage (Choi et al., 2014b; Lu et al., 2019; Shim et al., 2016; Tillmann et al., 2014; Zhang et al., 2019). However, it has disadvantages, such as limited application to sub-several micrometer-thick material and the necessity of a photo initiator (Bella et al., 2013; Choi et al., 2014a,b). Therefore, there is still strong demand for a quicker, room-temperature, scalable, and one-pot process to produce high-performance GPE-based LIBs for practical applications.

Radiation-based technology provides a promising way to prepare GPE-based LIBs. This technique offers discriminable characteristics including temperature-independent and additive-free chemical reaction, easy control over the chemical reaction, and scalability (Gupta et al., 2016). Exploiting these advantages, GPE-based LIBs were produced by γ-irradiation-induced gelation (Wang et al., 2017c). Recently, studies on the preparation of GPE-based LIBs by electron beam (EB) irradiation with a high linear energy transfer to enable much faster processing time have been reported and they exhibited potential as a scalable manufacturing technology while achieving comparable LIB performance to LE-based batteries (Sun et al., 2022; Cho et al., 2019; Guan et al., 2017). However, research through a combination of diverse radiation-sensitive liquid precursors and EB gelation is still needed in order to translate these advances to the industrial applications.

In this study, we demonstrate the in-situ formation of poly (vinylpyrrolidone)-based GPE (PVP-GPE) inside LIBs by quicker and more efficient EB irradiation. For this purpose, a radiation-sensitive GPE precursor solution was prepared by mixing 1-vinyl-2-pyrrolidone (VP) as a monomer and poly (ethylene glycol) diacrylate (PD) as a crosslinker with a commercial LE (1 M $LiClO_4$ in EC/DEC). To investigate the gelation behavior and the electrochemical properties of the resulting GPE, the precursor solution was irradiated by an EB at various absorbed doses. To demonstrate the feasibility of the PVP-GPE-based LIBs for practical use, coin-type LIBs were prepared by direct EB irradiation-induced gelation of a cell containing the precursor solution and its electrochemical performance in terms of charge–discharge characteristic and cyclic capability was evaluated.

2. Experiments

2.1. Materials

1-Vinyl-2-pyrrolidone (VP, >99.0%), poly (ethylene glycol) diacrylate (PEGDA, Mw = 700), lithium perchlorate ($LiClO_4$, 99.99%, battery grade), ethylene carbonate (EC, anhydrous, 99%) and diethyl carbonate (DEC, anhydrous, ≧ 99%) were purchased from Sigma-Aldrich. The LE (1 M $LiClO_4$ in EC/DEC (1/1, v/v) without any other additives was obtained from Welcos. The positive electrode formed by coating 95% $LiCoO_2$ active material onto an aluminum foil collector was purchased from MTI Korea Co., Ltd in Korea. The negative electrode, formed by coating a mixture of 94.5% composite graphite as the active material and styrene-butadiene rubber/carboxymethyl cellulose (SBR/CMC) binder onto copper foil, was purchased from MTI Korea Co., Ltd in Korea. A polypropylene/polyethylene (PP/PE) nonwoven separator was obtained from Nam Yang Nonwoven Fabric Co., Ltd (Ansan, Korea). All experiments were carried out in an argon atmosphere glove box (H_2O and $O_2 < 0.1$ ppm).

2.2. Preparation of PVP-GPE

The preparation of the precursor solution was carried out in an argon atmosphere glove box (H_2O and $O_2 < 0.1$ ppm) to minimize moisture and oxygen exposure. The precursor solution was composed of VP and PD dissolved in a LE consisting of 1 M $LiClO_4$ in a non-aqueous solution of EC:DEC with a volume ratio of 1:1. This solution was prepared at a weight ratio of 6 : 2: 92 (VP: PD: LE, wt %). After adding the precursor solution into propylene syringes (3 ml), the syringes were put into aluminum pouches and then thermally sealed to maintain the argon atmosphere of the glove box. To induce gelation of the precursor solution, the aluminum pouches were irradiated with an ELV-8 electron accelerator at a voltage of 2.5 MeV at Korea Atomic Energy Research Institute (Jeongeup, Korea) at room temperature. The EB current was 2.5 mA and the dose rate was 1 kGy/scan. The EB irradiation was performed while the tray was moved at 20 m/min. The absorbed doses were applied by increasing the number of scans from 1 to 8 kGy. Radiochromic B3 (BC 3000 batch) film dosimetry was performed according to ISO/ASTM 5149, and the uncertainty of the doses was less than 5%. The obtained PVP-GPE samples prepared from syringes were cut and used for characterization in terms of gel fraction, swelling degree, chemical structure, thermal decomposition, and compressive strength. The PVP-GPE samples were denoted as PVP-GPE-X, where X stands for the absorbed dose.

2.3. Characterization of the PVP-GPE

The gel fraction and swelling degree of the PVP-GPEs were measured gravimetrically method according to ASTM D2765-01. The gel fraction was determined by measuring the weight change of the dried GPEs before and after extraction. For extraction, 1 g of dried GPEs was placed into a 100 mesh stainless steel cage. The soluble part was extracted with EC/DEC solvent in a round bottom flask under vigorous magnetic stirring for 24 h. After the extraction, the samples were dried in a vacuum at 80 °C for 24 h. The gel fraction of the samples was calculated with the following equation:

$$\text{Gel fraction } (\%) = \frac{W_e}{W_o} \times 100 \quad (1)$$

where W_o and W_e are the weight of the dried GPEs before and after the solvent extraction, respectively. To measure the swelling degree, the GPEs were immersed in an EC/DEC solvent for 24 h at room temperature. After swelling, the samples were wiped with paper tissue to remove the excess solvent and then they were accurately weighed. The swelling degree was calculated as follows:

$$\text{Swelling degree } (\%) = \frac{W_s - W_o}{W_o} \times 100 \quad (2)$$

where W_s is the swollen weight of the GPEs after swelling in an EC/DEC solvent.

The chemical structure for the PVP-GPE was analyzed using attenuated total reflectance Fourier transform infrared spectrometry (ATR-FTIR, 640-IR, Varian). Absorbance spectra were obtained under the conditions of 32 scans at a resolution of 4 cm^{-1} within a range from 4000 to 700 cm^{-1}. Thermogravimetric analysis (TGA, Q 500, TA Instruments) was conducted to estimate the thermal stability of the PVP-GPE. The TGA analysis was conducted over a temperature range of 30–600 °C with a heating rate of 10 °C/min under a nitrogen atmosphere. The compressive stress and deformation of PVP-GPE were measured using the as-synthesized gel, which was cut into cylindrical pieces (diameter = 10 mm and height = 13 mm) by applying a sustained pressure with a speed of 5 mm/min using a texture meter (TA-XT2i, Surrey).

2.4. In-situ formation and electrochemical characterization of PVP-GPEs in coin-type LIBs

All electrochemical evaluations were performed with 2032 coin-type

cells and all PVP-GPEs in the coin cells for the electrochemical measurements were formed by EB-induced *in-situ* polymerization in the assembled state. Also, a separator (nonwoven fabric) was used to prevent direct contact between the two electrodes during *in-situ* polymerization in the assembled state. Ionic conductivities were measured through electrochemical impedance spectroscopy (EIS, SI-1287/SI-1260, Solartron) using symmetric coin cells of stainless steel (SS, φ = 16 mm)/PVP-GPE (Separator)/SS. The bulk resistance of the ionic conductivity was assessed by electrical impedance spectroscopy (EIS, SI-1260, Solartron). All the EIS measurements were performed using an alternative current signal with a potential amplitude of 10 mV and frequencies from 100 kHz to 0.1 Hz at 25 °C. The ionic conductivity was calculated as follows:

$$\sigma = \frac{t}{(R \times A)} \tag{3}$$

where t is the thickness of the PVP-GPE, R is the measured bulk resistance, and A is the contact area between the PVP-GPE and stainless steel. Linear sweep voltammetry (LSV) was carried out to confirm the electrochemical stability of the PVP-GPE at 25 °C by using an electrochemical analyzer (VersaSTAT4, AMETEK Inc.). The LSV curve was obtained using SS/PVP-GPE with nonwoven fabric/Li coin cells. The LSV was performed in a voltage range of 0 V–6 V at a scanning rate of 5 mV/s.

PVP-GPE-based LIBs were assembled in $LiCoO_2$/nonwoven fabric (separator)/graphite coin-type cells. After layering the negative electrode, separator, and positive electrode, the precursor solution was injected, and the cells were assembled. The assembled coin-type cells were EB-irradiated to induce gelation of the precursor solution. The surface morphology of the nonwoven fabric and free standing PVP GPE-2 was evaluated using a field emission scanning electron microscope (FE-SEM, JEOL, JSM-7500 F). Cycle performance testing of the PVP-GPE-based LIBs was conducted by using a charge/discharge test device (TOSCAT-3000, Toyo System). The cycle performance of each cell was evaluated under a rate of 0.1C from 3.0 V to 4.2 V at 25 °C.

3. Results and discussion

The one-pot preparation of poly (vinylpyrrolidone)-based GPE (PVP-GPE)-based LIBs by EB irradiation was sequentially performed as shown in Fig. 1. A VP monomer (possessing a good ion-transporting pyrrolidone group), PEGDA crosslinker (possessing di-acryl groups for gelation and a good ion-transporting ethylene glycol group), and $LiClO_4$ LE were selected as components for the precursor solutions (Arya and Sharma, 2017; Liu et al., 2020). The radiation-induced reactive precursor solution was prepared simply by mixing those selected components. To produce the PVP-GPE-based LIBs without any initiators or heat, the assembled coin-type cell containing the precursor solution was subjected to EB irradiation at room temperature. During the EB irradiation, the copolymerization of VP and PEGDA was initiated by radicals produced by radiolysis of the electrolyte, resulting in a solid-like crosslinked polymer network gel (Wang et al., 2017c). Unlike the conventional gelation techniques, this fast, room temperature, and initiator-free technique allows mass production while achieving the GPE characteristics.

3.1. EB-induced formation of the PVP-GPEs

To investigate the formation of PVP-GPE from its precursor solution by EB irradiation, the gel fraction and swelling degree of the PVP-GPEs prepared at various absorbed doses were measured, and the results are shown in Fig. 2. As seen in the figure, the PVP-GPE exhibited a gel fraction of 97% even at an absorbed dose of 1 kGy (corresponding to irradiation duration of 3 s) and 100% above the dose of 2 kGy, as reported in the literature (Wang et al., 2017c). To verify the crosslinking density of the as-prepared PVP-GPEs, the swelling degree of PVP-GPEs was measured and the results are shown in Fig. 2. As provided in Fig. 2, it can be seen that the swelling degree of the prepared GPEs was dependent on the absorbed dose. The swelling degree of PVP-GPE decreased from 190% to 92% with an increasing absorbed dose from 2 to 8 kGy (note that the PVP-GPE prepared at the absorbed dose of 1 kGy was not measured due to poor dimensional stability in a dry state). These results are attributed to the fact that the crosslinking density of PVP-GPE increased with an increase of absorbed dose, leading to a decrease in the swelling degree. Furthermore, as shown in the inset, the syringe containing the precursor solution showed typical liquid flow while the syringe irradiated at an absorbed dose of l kGy showed a gel-like flow. Therefore, these results indicate that the liquid precursor solution can be effectively converted to non-fluidic PVP-GPE by EB irradiation even at the absorbed dose of 1 kGy, and relatively good dimensional stability was obtained at absorbed doses above 2 kGy due to the formation of higher crosslinking density in the PVP-GPE ensuring mechanical robustness (Ryou et al., 2012).

To elucidate the formation of the PVP-GPEs from the precursor solution by EB irradiation, a chemical-structure analysis was performed using FT-IR. As shown in Fig. 3, the spectra of the VP monomer, PEGDA crosslinker, and LE (1 M $LiClO_4$ in EC/DEC) exhibited characteristic peaks at 1802 and 1773 cm^{-1} (C═O in EC electrolyte), 1746 cm^{-1} (C═O in DEC electrolyte) (Seo et al., 2015), 1695 cm^{-1} (C═O in VP) (Maheswari et al., 2014), 1633 cm^{-1} (C═C in PEGDA) (Duan et al.,

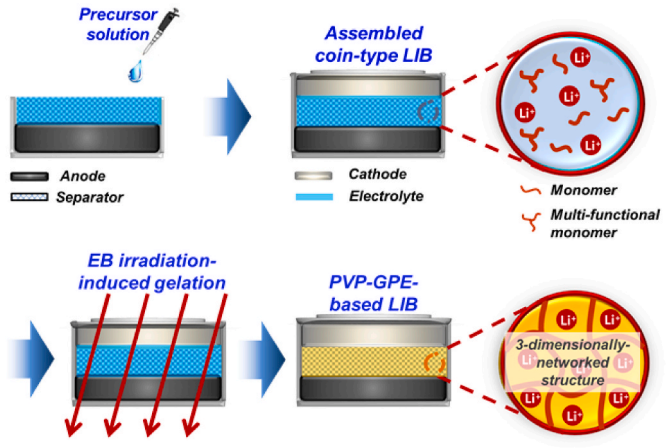

Fig. 1. Schematic diagram of fabrication of PVP-GPE-based LIBs by EB irradiation.

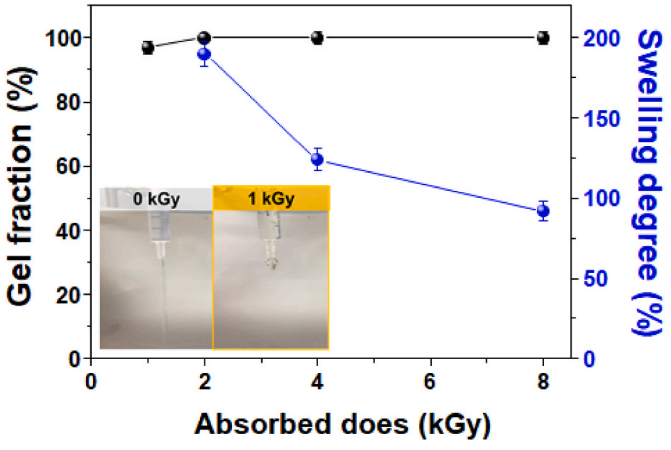

Fig. 2. Gel fraction and swelling degree of PVP-GPE as a function of the absorbed dose (the inset shows photographs of the PVP-GPE precursor solution before and after EB irradiation at an absorbed dose of 1 kGy).

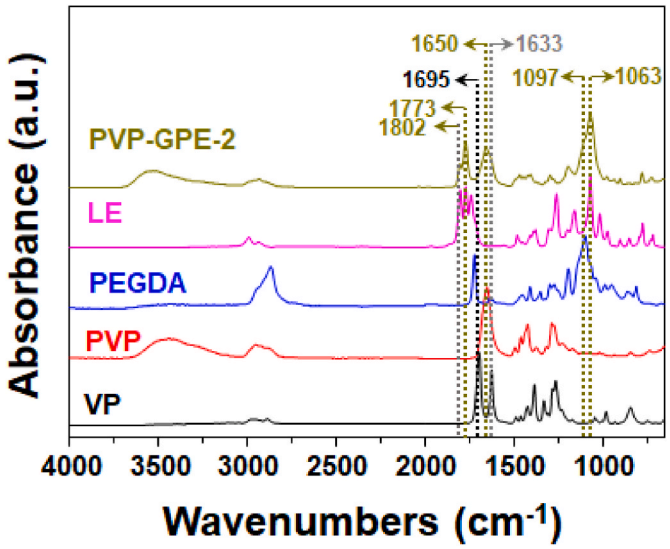

Fig. 3. FT-IR spectra of the VP monomer, PEGDA cross-linker, LE, and PVP-GPE-2.

2018), 1625 cm^{-1} (C═C in VP) (Maheswari et al., 2014), 1097 cm^{-1} (C–O in PEGDA) (Florkiewicz et al., 2021), and 1063 cm^{-1} (ClO_4^- in $LiClO_4$) (Chitra et al., 2020). On the other hand, a distinct peak in the PVP-GPE spectrum (corresponding to C═O in the PVP spectrum) appeared at 1650 cm^{-1} along with the characteristic peaks of PEGDA crosslinkers and $LiClO_4$ in EC/DEC electrolytes. This distinct peak was likely due to the lower wavenumber shift of C═O in the VP spectrum by polymerization (Liu et al., 2013). This reveals that polymerization of VP and PEGDA occurred in the presence of $LiClO_4$ LE during the EB irradiation, although the disappearance of the double bond was difficult to prove.

To investigate the thermal stability (considered a key issue to secure LIB safety), the thermal decomposition behavior of LE and PVP-GPE-2 (prepared at the absorbed dose of 2 kGy) was analyzed by TGA. As shown in Fig. 4, LE exhibited two major weight losses in the temperature range of 30–180 °C (attributed to vaporization of EC/DEC solvent) and 450–500 °C (corresponding to decomposition of $LiClO_4$ as shown in its TGA curve), respectively (Wang et al., 2017c). On the other hand, the main weight loss of PVP-GPE-2 began at 100 °C, which is a higher temperature in comparison to that of LE. This result indicates that PVP-GPE has improved thermal stability in comparison with

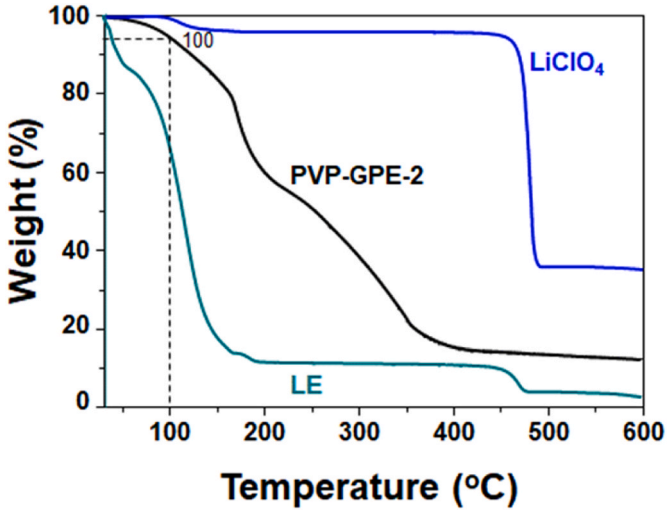

Fig. 4. TGA curves of LE, $LiClO_4$, and PVP-GPE-2.

conventional LE, stemming from the formation of the thermal-resistant crosslinked PVP structure (Choi et al., 2014b). To further examine the safety-related flammability of PVP-GPEs, an ignition test was performed, and a photograph of the flammable behavior is shown in Fig. 5. As seen in Fig. 5(a), upon exposure to the flame, the LE-based nonwoven separator was immediately burned, and the flame was very large due to the high flammability of the combustible EC/DEC solvents. However, both PVP-GPE-2 and -4 combusted after relatively longer exposure time. These results demonstrate the better flame-retardant property of PVP-GPE in comparison to that of the conventional LE.

To evaluate the mechanical robustness of PVP-GPEs, a compression test was performed. As shown in Fig. 6, the compressive strength of the PVP-GPEs increased from 2.4 kPa to 4.6 kPa with an increasing absorbed dose, whereas their deformation decreased from 74% to 64%. This reveals that the PVP-GPE prepared even at an absorbed dose of 2 kGy has sufficient mechanical robustness to retain its cylindrical shape under compression, as shown in the inset in Fig. 6, and the degree of robustness depended on the absorbed dose. This can be ascribed to the fact that a higher absorbed dose results in denser crosslinked structures, leading to improved mechanical robustness of PVP-GPEs (Xu et al., 2018). Overall, EB irradiation at an absorbed dose of above 2 kGy (corresponding to irradiation time of only 6 s) enabled the formation of self-standing and thermally-stable PVP-GPEs (from the precursor solution containing 92 wt% LEs). Moreover, the characteristics of PVP-GPEs can be simply adjusted by the absorbed dose (Park et al., 2023).

3.2. Electrochemical characterization of PVP-GPEs

To investigate whether ion conductivity critically influences the LIB performance, the bulk resistances of PVP-GPEs and the corresponding ion conductivity were measured using an EIS, and the results are shown in Fig. 7 and Table 1. As seen in the impedance spectra (Fig. 7), the bulk resistance of PVP-GPEs exhibited a tendency to increase with an increasing absorbed dose. As summarized in Table 1 listing the ion conductivity calculated from the bulk resistance, the ion conductivity of PVP-GPE-2 is 2.03×10^{-3} S/cm, which is comparable to that of a LE (2.78×10^{-3} S/cm) reported in the literature (Saikia and Kumar, 2004). However, PVP-GPE-4 and -8 showed lower ion conductivity of 1.74×10^{-3} S/cm and 8.03×10^{-4} S/cm, respectively. These results indicate that, even though it was almost completely crosslinked, PVP-GPE-2 at the lower absorbed dose of 2 kGy facilitates ion transport as much as LE, but the formation of much denser crosslinked networks in PVP-GPE at

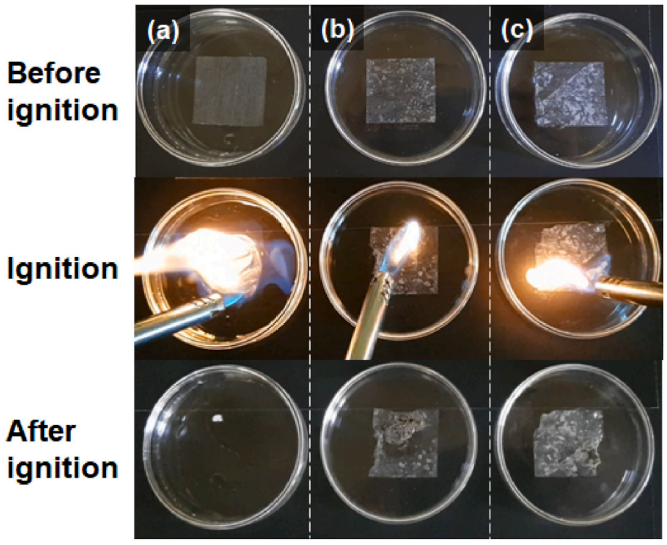

Fig. 5. Photographs for the flammable behavior of (a) LE-, (b) PVP-GPE-2-, and (c) PVP-GPE-4-based nonwoven separator.

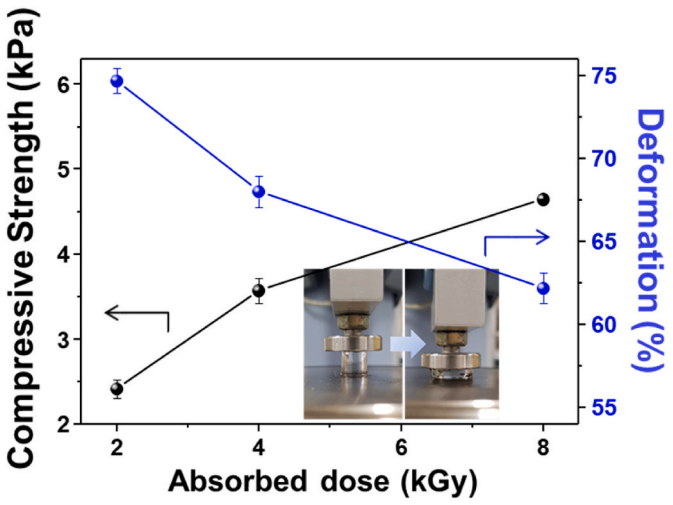

Fig. 6. Compressive strength and deformation of PVP-GPE-2, -4, and -8 (the inset image shows the compressive strength measurement of PVP-GPE-2).

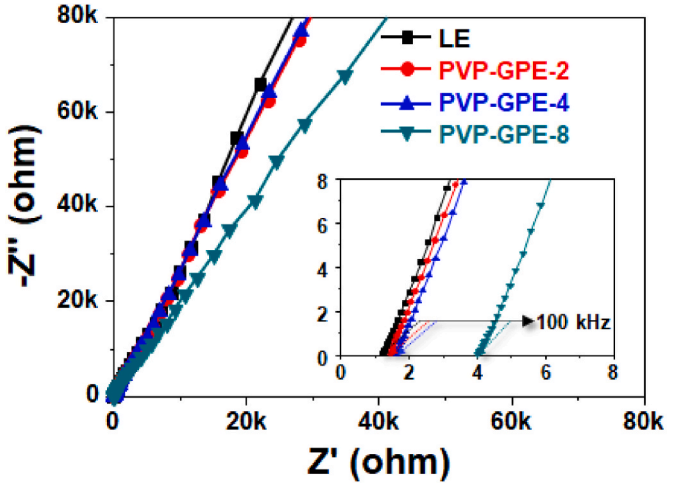

Fig. 7. Impedance spectra of LE, PVP-GPE-2, -4, and -8.

Table 1
Ionic conductivity of LE, PVP-GPE-2, -4, and -8.

Electrolyte	Ionic conductivity (S/cm)
LE	2.78×10^{-3}
PVP-GPE-2	2.03×10^{-3}
PVP-GPE-4	1.74×10^{-3}
PVP-GPE-8	8.03×10^{-4}

the higher absorbed dose deteriorates the ion transport, leading to a reduction in the ion conductivity (Liu et al., 2017).

To examine the electrochemical stability window of PVP-GPE as an indicator for the possibility of practical use, a linear sweep voltammetry analysis was performed, and the results are presented in Fig. 8. As seen, PVP-GPE-2, -4, and, -8 all showed no change in current density within a voltage range from 2.0 to 4.7 V, similar to the electrochemical stability window of LE. This may be ascribed to the high portion of LE in the PVP GPEs (Li et al., 2017). These results indicate that all the PVP-GPE samples could be as electrochemically stable as LE at the given voltage (fulfilling the required operating voltage range of a commercial LIB). Therefore, it is ascertained from these overall analytic results that the crosslinked networked PVP-GPE (with better thermal stability and comparable ionic conductivity in comparison to the conventional LE)

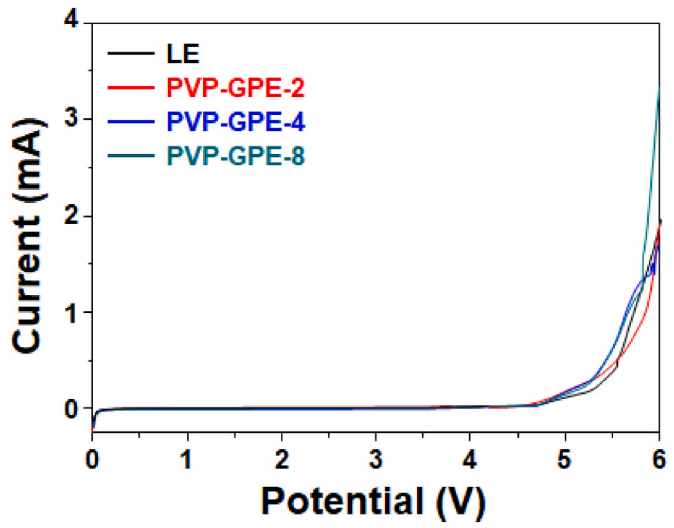

Fig. 8. Linear sweep voltammogram of LE, PVP-GPE-2, -4, and -8.

was quickly prepared by EB-induced copolymerization of VP and PD in the presence of $LiClO_4$ electrolyte without a photo initiator or high temperature. Taking into consideration the ion conductivity and electrochemical stable voltage window, EB irradiation was performed at absorbed doses of 2 and 4 kGy to further investigate the practical coin-type cell performance.

3.3. In-situ formation and electrochemical performance of PVP-GPE in coin-type LIB cells

To confirm the in-situ formation of PVP-GPE through direct EB irradiation of coin-type cells, a PVP-GPE-2-based nonwoven separator (prepared in an assembled coin-type state without electrode at the absorbed dose of 2 kGy) and a LE-based separator were observed by FE-SEM. As shown in Fig. 9(a), the LE-based separator exhibited a typical nonwoven porous structural morphology. On the other hand, as seen in Fig. 9(b), the PVP-GPE-2-based separator showed a filled nonwoven structural morphology. This result implies that the precursor solution inside the nonwoven separator of the assembled coin-type cell can be successfully transformed into a solid-like PVP-GPE by EB irradiation even in an assembled coin cell, as reported with regard to in-situ γ–ray-induced formation of GPE (Wang et al., 2017c).

To practically demonstrate the feasibility of in-situ PVP-GPE-based LIBs, coin-type graphite/$LiCoO_2$ cells were fabricated with LE-, PVP-GPE-2-, and -4-based nonwoven separators, and the results are shown in Fig. 10. As seen in the charge-discharge profiles (Fig. 10(a)), the PVP-GPE-2-based cell exhibited initial discharge capacity of 133 mAh/g, which is comparable to that with a LE (135 mAh/g). However, the PVP-GPE-4-based cells showed a much lower initial discharge capacity. This improved discharge capacity of PVP-GPE-2 is ascribed to the higher ion conductivity in comparison to that of PVP-GPE-4. Furthermore, as shown in the lifetime cycling performance (Fig. 10(b)), the PVP-GPE-2-based cell delivered a discharge capacity of 92 mAh/g after 50 cycles, corresponding to a capacity retention of about 69% with an overall Coulombic efficiency of 98%. This performance was close to that of a LE-based cell (98 mAh/g) corresponding to a capacity retention of 72% with an overall Coulombic efficiency of 98%. However, the capacity retention of the PVP-GPE-4-based cells was much lower than that with PVP-GPE-2 due to the relatively lower ionic conductivity at the higher absorbed dose. This indicates that chemically-crosslinked PVP-GPE-based LIBs (comparable to that with a LE) can be achieved by ambient and quick fabrication of in-situ EB-induced gelation. In addition, we believe that this in-situ EB-induced gelation strategy in combination with various precursor formulations and functionalization of the

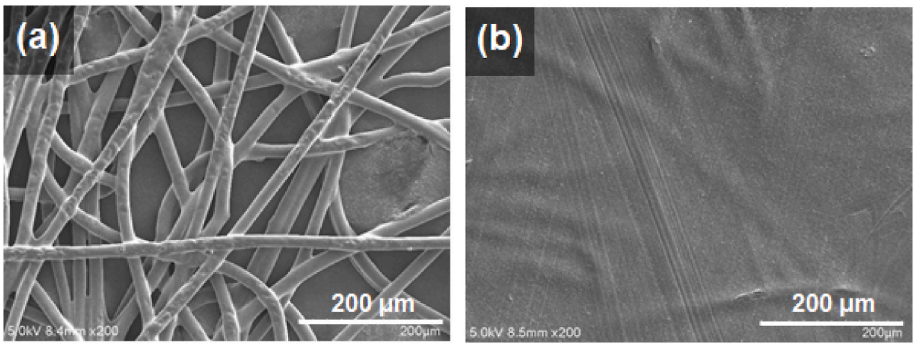

Fig. 9. FE-SEM images of (a) LE- and (b) PVP-GPE-2-based nonwoven separators independently prepared in an assembled coin-type state without electrodes.

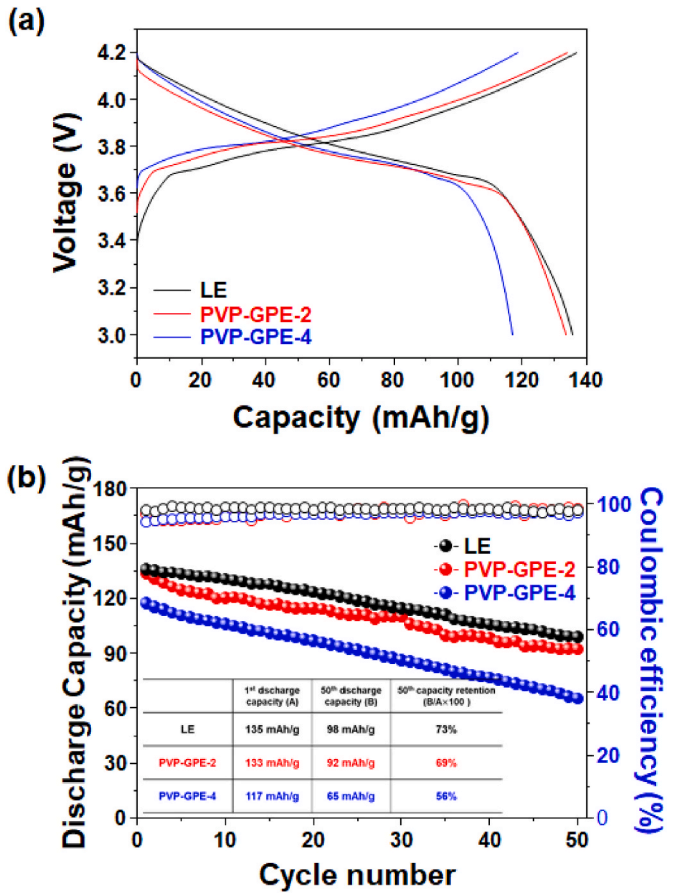

Fig. 10. Electrochemical performance of $LiCoO_2$/graphite coin-type cells with liquid electrolyte-, PVP-GPE-2, and -4-based separators: (a) first charge-discharge curves and (b) cycle performance curves (the inset shows the 50^{th} discharge capacity retention calculated from the 1^{st} and 50^{th} discharge capacities).

separator to control the ion conductivity can further produce reasonable performance and safe solid-like GPE-based LIBs.

4. Conclusion

PVP-GPE-based LIBs were successfully fabricated by direct EB irradiation gelation of a precursor inside coin-type LIB cells. The analytical results in terms of radiation-induced gel behavior, thermal stability, and electrochemical properties revealed that PVP-GPE was created by EB irradiation at an absorbed dose of 2 kGy (corresponding to irradiation duration of 6 s). The resulting PVP-GPE exhibited a gel fraction of 100%, thermal stability, a good electrochemically stable voltage window (2.0–4.7 V), and good ionic conductivity (2.03×10^{-3} S/cm). As a result, the coin-type LIB cell fabricated with PVP-GPE-2 exhibited an initial discharge capacity of 133 mAh/g, and its capacity retention at a cycle number of 50 was 69%, which is comparable to that with a LE (135 mAh/g and 72%). These findings clearly demonstrate that this simple, quick, heat-free, and scalable EB-based strategy is a feasible approach for the mass production of more stable and reasonable performance GPE-based LIBs.

CRediT authorship contribution statement

Joon-Yong Sohn: Conceptualization, Investigation, Methodology, Writing-original draft. **Ji Hoon Choi:** Investigation, Methodology. **Pyeong-Wook Kim:** Investigation, Methodology. **In-Tae Hwang:** Investigation, Methodology. **Junhwa Shin:** Investigation, Methodology. **Chan-Hee Jung:** Investigation, Visualization, Writing-review & editing. **Young-Moo Lee:** Investigation, Writing-review & editing.

Declaration of competing interest

The authors declare that they have no known competing financial interests or personal relationships that could have appeared to influence the work reported in this paper.

Data availability

No data was used for the research described in the article.

Acknowledgements

This work was supported by Korea Atomic Energy Research Institute (KAERI) Institutional Program (Project No. 523230–23).

References

Arya, A., Sharma, A.L., 2017. Polymer electrolytes for lithium ion batteries: a critical study. Ionics 23, 497–540. https://doi.org/10.1007/s11581-016-1908-6.

Bella, F., Ozzello, E.D., Bianco, S., Bongiovanni, R., 2013. Photo-polymerization of acrylic/methacrylic gel–polymer electrolyte membranes for dye-sensitized solar cells. Chem. Eng. J. 225, 873–879. https://doi.org/10.1016/j.cej.2013.04.057.

Cavers, H., Molaiyan, P., Abdollahifar, M., Lassi, U., Kwade, A., 2022. Perspectives on improving the safety and sustainability of high voltage lithium-ion batteries through the electrolyte and separator region. Adv. Energy Mater. 12, 2200147 https://doi.org/10.1002/aenm.202200147.

Chen, K.-S., Balla, I., Luu, N.S., Hersam, M.C., 2017. Emerging opportunities for two-dimensional materials in lithium-ion batteries. ACS Energy Lett. 2, 2026–2034. https://doi.org/10.1021/acsenergylett.7b00476.

Chen, Y., Kang, Y., Zhao, Y., Wang, L., Liu, J., Li, Y., Liang, Z., He, X., Li, X., Tavajohi, N., Li, B., 2021. A review of lithium-ion battery safety concerns: the issues, strategies, and testing standards. J. Energy Chem. 59, 83–99. https://doi.org/10.1016/j.jechem.2020.10.017.

Cheng, X., Pan, J., Zhao, Y., Liao, M., Peng, H., 2018. Gel polymer electrolytes for electrochemical energy storage. Adv. Energy Mater. 8, 1702184 https://doi.org/10.1002/aenm.201702184.

Chitra, R., Sathya, P., Selvasekarapandian, S., Meyvel, S., 2020. Synthesis and characterization of iota-carrageenan biopolymer electrolyte with lithium perchlorate and succinonitrile (plasticizer). Polym. Bull. 77, 1555–1579. https://doi.org/10.1007/s00289-019-02822-y.

Cho, Y.-G., Hwang, C., Cheong, D.S., Kim, Y.-S., Song, H.-K., 2019. Gel/solid polymer electrolytes characterized by in situ gelation or polymerization for electrochemical energy systems. Adv. Mater. 31, 1804909 https://doi.org/10.1002/adma.201804909.

Choi, J.-A., Yoo, J.-H., Yoon, W.Y., Kim, D.-W., 2014a. Cycling characteristics of lithium powder polymer cells assembled with cross-linked gel polymer electrolyte. Electrochim. Acta 132, 1–6. https://doi.org/10.1016/j.electacta.2014.03.119.

Choi, K.-H., Cho, S.-J., Kim, S.-H., Kwon, Y.H., Kim, J.Y., Lee, S.-Y., 2014b. Thin, deformable, and safety-reinforced plastic crystal polymer electrolytes for high-performance flexible lithium-ion batteries. Adv. Funct. Mater. 24, 44–52. https://doi.org/10.1002/adfm.201301345.

Deng, K., Zeng, Q., Wang, D., Liu, Z., Wang, G., Qiu, Z., Zhang, Y., Xiao, M., Meng, Y., 2020. Nonflammable organic electrolytes for high-safety lithium-ion batteries. Energy Storage Mater. 32, 425–447. https://doi.org/10.1016/j.ensm.2020.07.018.

Duan, H., Yin, Y.-X., Zeng, X.-X., Li, J.-Y., Shi, J.-L., Shi, Y., Wen, R., 2018. In-situ plasticized polymer electrolyte with double-network for flexible solid-state lithium-metal batteries. Energy Storage Mater. 10, 85–91. https://doi.org/10.1016/J.ensm.2017.06.017.

Duan, J., Tang, X., Dai, H., Yang, Y., Wu, W., Wei, X., Huang, Y., 2020. Building safe lithium-ion batteries for electric vehicles: a review. Electrochem. Energy Rev. 3, 1–42. https://doi.org/10.1007/s41918-019-00060-4.

Florkiewicz, W., Slota, D., Placek, A., Pluta, K., Tyliszczak, B., Douglas, T.E.L., Sobczak-Kupiec, A., 2021. Synthesis and characterization of polymer-based coatings modified with bioactive ceramic and bovine serum albumin. J. Funct. Biomater. 12, 21. https://doi.org/10.3390/jfb12020021.

Guan, J., Li, Y., Li, J., 2017. Stretchable ionic-liquid-based gel polymer electrolytes for lithium-ion batteries. Ind. Eng. Chem. Res. 56, 12456–12463. https://doi.org/10.1021/acs.iecr.7b03387.

Gupta, B., Kumar, N., Panda, K., Melvin, A.A., Joshi, S., Dash, S., Tyagi, A.K., 2016. Effective noncovalent functionalization of poly(ethylene glycol) to reduced graphene oxide nanosheets through γradiolysis for enhanced lubrication. J. Phys. Chem. C 120, 2139–2148. https://doi.org/10.1021/acs.jpcc.5b08762.

Kim, T., Song, W., Son, D.-Y., Ono, L.K., Qi, Y., 2019. Lithium-ion batteries: outlook on present, future, and hybridized technologies. J. Mater. Chem. 7, 2942–2964. https://doi.org/10.1039/c8ta10513h.

Kuo, P.-L., Tsao, C.-H., Hsu, C.-H., Chen, S.-T., Hsu, H.-M., 2016. A new strategy for preparing oligomeric ionic liquid gel polymer electrolytes for high-performance and nonflammable lithium ion batteries. J. Membr. Sci. 499, 462–469. https://doi.org/10.1016/j.memsci.2015.11.007.

Lee, A.S.S., Lee, J.H., Lee, J.-C., Hong, S.M., Hwang, S.S., 2014. Novel polysilsesquioxane hybrid polymer electrolytes for lithium ion batteries. J. Mater. Chem. 2, 1277–1283. https://doi.org/10.1039/c3ta14290f.

Li, W., Pang, Y., Liu, J., Liu, G., Wang, Y., Xia, Y., 2017. A PEO-based gel polymer electrolyte for lithium ion batteries. RSC Adv. 7, 23494 https://doi.org/10.1039/c7ra02603j.

Liu, M., Wang, Y., Li, M., Li, G., Li, B., Zhang, S., Ming, H., Qiu, J., Chen, J., Zhao, P., 2020. A new composite gel polymer electrolyte based on matrix of PEGDA with high ionic conductivity for lithium-ion batteries. Electrochim. Acta 354, 136622. https://doi.org/10.1016/j.electacta.2020.136622.

Liu, W., Zhang, X.K., Wu, F., Xiang, Y., 2017. A study on PVDF-HFP gel polymer electrolyte for lithium-ion batteries. IOP Conf. Ser. Mater. Sci. Eng. 213, 012036 https://doi.org/10.1088/1757-899X/213/1/012036.

Liu, X., Tong, W., Wu, Z., Jiang, W., 2013. Poly(N-vinylpyrrolidone)-grafted poly (dimethylsiloxane) surfaces with tunable microtopography and anti-biofouling properties. RSC Adv. 3, 4716. https://doi.org/10.1039/c3ra23069d.

Lu, Y., He, K.-W., Zhang, S.-J., Zhou, Y.-X., Wang, Z.-B., 2019. UV-curable-based plastic crystal polymer electrolyte for high-performance all-solid-state Li-ion batteries. Ionics 25, 1607–1615. https://doi.org/10.1007/s11581-018-2788-8.

Lv, P., Li, Y., Wu, Y., Liu, G., Liu, H., Li, S., Tang, C., Mei, J., Li, Y., 2018. Robust succinonitrile-based gel polymer electrolyte for lithium-ion batteries withstanding mechanical folding and high temperature. ACS Appl. Mater. Interfaces 10, 25384–25392. https://doi.org/10.1021/acsami.8b06800.

Ma, C., Cui, W., Liu, X., Ding, Y., Wang, Y., 2022. In situ preparation of gel polymer electrolyte for lithium batteries: progress and perspectives. InfoMat 4, e12232. https://doi.org/10.1002/inf2.12232.

Maheswari, B., Babu, P.E.J., Agarwal, M., 2014. Role of N-vinyl-2-pyrrolidinone on the thermoresponsive behavior of PNIPAm hydrogel and its release kinetics using dye and vitamin-B12 as model drug. J. Biomater. Sci. Polym. Ed. 25, 269–286. https://doi.org/10.1080/09205063.2013.854149.

Oh, S., Kim, D.W., Lee, C., Lee, M.-H., Kang, Y., 2011. Poly(vinylpyridine-co-styrene) based in situ cross-linked gel polymer electrolyte for lithium-ion polymer batteries. Electrochim. Acta 57, 46–51. https://doi.org/10.1016/j.electacta.2011.05.029.

Park, S., Sohn, J.-Y., Hwang, I.-T., Shin, J., Yun, J.-M., Eom, K., Shin, K., Lee, Y.-M., Jung, C.-H., 2023. In-situ preparation of gel polymer electrolytes in a fully-assembled lithium ion battery through deeply-penetrating high-energy electron beam irradiation. Chem. Eng. J. 452, 139339 https://doi.org/10.1016/j.cej.2022.139339.

Rao, M., Geng, X., Liao, Y., Hu, S., Li, W., 2012. Preparation and performance of gel polymer electrolyte based on electrospun polymer membrane and ionic liquid for lithium ion battery. J. Membr. Sci. 399–400, 37–42. https://doi.org/10.1016/j.memsci.2012.01.021.

Ryou, M.H., Lee, Y.M., Cho, K.Y., Han, G.B., Lee, J.N., Lee, D.J., Choi, J.W., Park, J.K., 2012. A gel polymer electrolyte based on initiator-free photopolymerization for lithium secondary batteries. Electrochim. Acta 60, 23–30. https://doi.org/10.1016/j.electacta.2011.10.072.

Saikia, D., Kumar, A., 2004. Ionic conduction in P(VDF-HFP)/PVDF–(PC + DEC)–$LiClO_4$ polymer gel electrolytes, Electrochim. Acta 49, 2581–2589. https://doi.org/10.1016/j.electacta.2004.01.029.

Schmuch, R., Wagner, R., Hörpel, G., Placke, T., Winter, M., 2018. Performance and cost of materials for lithium-based rechargeable automotive batteries. Nat. Energy 3, 267–278. https://doi.org/10.1038/s41560-018-0107-2.

Seo, D.M., Reininger, M., Kutcher, M., Redmond, K., Euler, W.B., Lucht, B.L., 2015. Role of mixed solvation and ion pairing in the solution structure of lithium ion battery electrolytes. J. Phys. Chem. C 119, 14038–14046. https://doi.org/10.1021/acs.jpcc.5bo3694.

Service, R.F., 2019. Lithium-ion battery development takes Novel. Science 366, 292. https://doi.org/10.1126/science.366.6463.292.

Shi, J., Hu, H., Xia, Y., Liu, Y., Liu, Z., 2014. Polyimide matrix-enhanced cross-linked gel separator with three-dimensional heat-resistance skeleton for high-safety and high-power lithium ion batteries. J. Mater. Chem. 2, 9134–9141. https://doi.org/10.1039/c4ta00808a.

Shim, J., Kim, H.J., Kim, B.G., Kim, Y.S., Kim, D.G., Lee, J.C., 2017. 2D boron nitride nanoflakes as a multifunctional additive in gel polymer electrolytes for safe, long cycle life and high rate lithium metal batteries. Energy Environ. Sci. 10, 1911–1916. https://doi.org/10.1039/c7ee01095h.

Shim, J., Lee, J.S., Lee, J.H., Kim, H.J., Lee, J.-C., 2016. Gel polymer electrolytes containing anion-trapping boron moieties for lithium-ion battery applications. ACS Appl. Mater. Interfaces 8, 27740–27752. https://doi.org/10.1021/acsami.6b09601.

Song, J.Y., Wang, Y.Y., Wan, C.C., 1999. Review of gel-type polymer electrolytes for lithium-ion batteries. J. Power Sources 77, 183–197. https://doi.org/10.1016/S0378-7753(98)00193-1.

Sun, M., Zeng, Z., Hu, W., Sheng, K., Wang, Z., Han, Z., Peng, L., Yu, C., Cheng, S., Fan, M., Huang, J., Xie, J., 2022. Scalable fabrication of solid-state batteries through high-energy electronic beam. Chem. Eng. J. 431, 134323 https://doi.org/10.1016/j.cej.2021.134323.

Tillmann, S.D., Isken, P., Lex-Balducci, A., 2014. Gel polymer electrolyte for lithium-ion batteries comprising cyclic carbonate moieties. J. Power Sources 271, 239–244. https://doi.org/10.1016/j.jpowsour.2014.07.185.

Wang, F., Varenne, F., Ortiz, D., Pinzio, V., Mostafavi, M., Sophie, L.C., 2017. Degradation of an ethylene carbonate/diethyl carbonate mixture by using ionizing radiation. ChemPhysChem 18, 2799–2806. https://doi.org/10.1002/cphc.201700320.

Wang, X., Zhu, H., Gaetan, M.A.G., Yunis, R., Douglas, R.M., David, M., Aninda, J.B., Patrick, C.H., Maria, F., 2017. Preparation and characterization of gel polymer electrolytes using poly(ionic liquids) and high lithium salt concentration ionic liquids. J. Mater. Chem. 5, 23844–23852. https://doi.org/10.1039/c7ta08233a.

Wang, Y., Qiu, J., Peng, J., Li, J., Zhai, M., 2017. One-step radiation synthesis of gel polymer electrolytes with high ionic conductivity for lithium-ion batteries. J. Mater. Chem. 5, 12393–12399. https://doi.org/10.1039/c7ta02291c.

Woo, H.-S., Moon, Y.-B., Seo, S., Lee, H.-T., Kim, D.-W., 2018. Semi-interpenetrating polymer network composite gel electrolytes employing vinyl-functionalized silica for lithium−oxygen batteries with enhanced cycling stability. ACS Appl. Mater. Interfaces 10, 687–695. https://doi.org/10.1021/acsami.8b06800.

Xu, D., Jin, J., Chen, C., Wen, Z., 2018. From nature to energy storage: a novel sustainable 3D cross-linked chitosan−PEGGE-based gel polymer electrolyte with excellent lithium-ion transport properties for lithium batteries. ACS Appl. Mater. Interfaces 10, 38526–38537. https://doi.org/10.1021/acsami.8b15247.

Xu, K., 2014. Electrolytes and interphases in li-ion batteries and beyond. Chem. Rev. 114, 11503–11618. https://doi.org/10.1021/cr500003w.

Zhang, S.Z., Xia, X.H., Xie, D., Xu, R.C., Xu, Y.J., Xia, Y., Wu, J.B., Yao, Z.J., Wang, X.L., 2019. Facile interfacial modification via in-situ ultraviolet solidified gel polymer electrolyte for high-performance solid-state lithium ion batteries. J. Power Sources 409, 31–37. https://doi.org/10.1016/j.jpowsour.2018.10.088.

Zheng, J., Li, X., Yu, Y., Zhen, X., Song, Y., Feng, X., Zhao, Y., 2014. Cross-linking copolymers of acrylates' gel electrolytes with high conductivity for lithium-ion batteries. J. Solid State Electrochem. 18, 2013–2018. https://doi.org/10.1007/s10008-014-2438-7.

Zhou, D., He, Y.-B., Cai, Q., Qin, X., Li, B., Du, H., Yang, Q.-H., Kang, F., 2014. Investigation of cyano resin-based gel polymer electrolyte: in situ gelation mechanism and electrode–electrolyte interfacial fabrication in lithium-ion battery. J. Mater. Chem. 2, 20059–20066. https://doi.org/10.1039/c4ta04504a.

Zhou, D., He, Y.B., Liu, R., Liu, M., Du, H., Li, B., Cai, Q., Yang, Q.-H., Kang, F., 2015. In situ synthesis of a hierarchical all-solid-state electrolyte based on nitrile materials for high-performance lithium-ion batteries. Adv. Energy Mater. 5, 1500353 https://doi.org/10.1002/aenm.201500353.

Zhu, M., Lan, J., Tan, C., Sui, G., Yang, X., 2016. Degradable cellulose acetate/poly-L-lactic acid/halloysite nanotube composite nanofiber membranes with outstanding performance for gel polymer electrolytes. J. Mater. Chem. 4, 12136–12143. https://doi.org/10.1039/C6TA05207J.

Zhu, Y.S., Xiao, S.Y., Li, M.X., Chang, Z., Wang, F.X., Gao, J., Wu, Y.P., 2015. Natural macromolecule based carboxymethyl cellulose as a gel polymer electrolyte with adjustable porosity for lithium ion batteries. J. Power Sources 288, 368–375. https://doi.org/10.1016/j.jpowsour.2015.04.117.

Zubi, G., Dufo-López, R., Carvalho, M., Pasaoglu, G., 2018. The lithium-ion battery: state of the art and future perspectives. Renew. Sustain. Energy Rev. 89, 292–308. https://doi.org/10.1016/j.rser.2018.03.002.